AIAA SciTech Forum
January 3-7, 2022, San Diego, CA & Virtual
AIAA SCITECH 2022 Forum

10.2514/6.2022-2371

Time Series Classification within a Rotating Detonation Engine through Deep Convolutional Neural Networks applied to High-Speed Pressure and Ion Probe Data

Kristyn B. Johnson[1], and Donald H. Ferguson[2]
National Energy Technology Laboratory, Morgantown, WV 26507, USA

Andrew C. Nix[3]
West Virginia University, Mechanical and Aerospace Engineering, Morgantown, WV 26505, USA

Studied as a means for improved gas turbine efficiency through the accomplishment of continuous detonation, rotating detonation engines (RDEs) are of great interest to the pressure gain combustion research community. Through the development of cooling strategies, such as that of the currently studied water-cooled RDE at the National Energy Technology Laboratory (NETL), experimental operational times continue to be extended. Longer operating time is vital to the study of mode stability, quasi-steady heat transfer, and downstream turbine integration, all of which contribute to the final goal of technology maturation and industrial implementation. As RDE technology matures towards this stage, diagnostic techniques must also be advanced toward real-time capabilities. Due to the timescale of observable detonation behaviors, time series sensor data is studied for an experimental RDE at high sampling rates exceeding 250 kHz, which results in large volumes of data. This data most often requires post-processing deterministic methods, which will likely never achieve real-time diagnostic speeds. In an effort to address this issue, a deep learning approach to time series classification (TSC) is proposed. Pressure and ion probe data collected near the RDE detonation plane is recorded and used to create 8 datasets of varying sample lengths: 200, 500, and 700 samples. These datasets, 6 univariate and 2 multivariate, are filtered and labeled according to the wave mode detected by simultaneous down-axis imaging. Further examining the effects of a TSC approach, each dataset is used to train three deep neural network architectures, an encoder, a fully convolutional network (FCN), and a residual network (ResNet), resulting in 24 uniquely trained networks. Networks are randomly initialized five times and trained over 250 epochs each time. The incremental network that minimizes loss is chosen as the finalized network. Among the results of the 24 finalized networks, shorter data lengths and multivariate data sets show the highest performances. The best performing individual network is a multivariate encoder, while ResNet achieves the highest overall average rank among the three architectures. According to the goal of the current study, which is to develop a component of a real-time RDE diagnostic, classification time is of high importance in the selection of a preferred network. Therefore, an FCN trained on a multivariate dataset with a data length of 200 samples is selected as a preferred network that is believed to best optimize classification time alongside validation accuracy, being 28.76 msec and 91.36% respectively. The chosen network's classification time corresponds to a classification rate of nearly 35 Hz, outperforming the speed of an RDE image classification network developed in a previous study by the current authors. It is believed that a reduced data acquisition time associated with the low dimensionality of time series data will enhance the viability of the TSC method and its contribution to a real-time RDE diagnostic.

[1] Post-Graduate Research Associate, WVU PhD Student, AIAA Member, kristyn.johnson@netl.doe.gov
[2] Senior Research Engineer, Corresponding, AIAA Member, donald.ferguson@netl.doe.gov
[3] Associate Professor, AIAA Member, andrew.nix@mail.wvu.edu

Nomenclature

AB	=	Allen Bradley
CAML	=	Center for Artificial Intelligence and Machine Learning
CR	=	counter-rotating
CTAP	=	capillary tube average pressure
CW	=	clockwise
CCW	=	counterclockwise
CNN	=	convolutional neural network
DNN	=	deep neural network
FCN	=	fully convolutional network
fps	=	frames per second
GAP	=	global average pooling
ITP	=	infinite tube pressure
LECTR	=	Low Emission Combustor Test and Research facility
NETL	=	National Energy Technology Laboratory
NLP	=	natural language processing
NN	=	nearest neighbor
ORISE	=	Oak Ridge Institute for Science and Education
PGC	=	pressure gain combustion
PReLU	=	parametric rectified linear unit
R-CNN	=	region-based convolutional neural network
RDE	=	rotating detonation engine
ReLU	=	rectified linear unit
RMSE	=	root-mean-square error
SGD	=	stochastic gradient descent
SVM	=	support vector machine
TSC	=	time series classification
UV	=	ultraviolet
YOLO	=	You Only Look Once

Variables:

$A_{3.1}$	=	air injector area
$A_{3.2}$	=	combustor channel area
A_8	=	nozzle exit area
x_i	=	data point *i*
$x_{i,Z}$	=	Z-normalized data point *i*

Greek Variables:

μ_{global}	=	global mean
σ_{global}	=	global standard deviation

Introduction

Rotating detonation engines (RDEs) offer, through pressure gain combustion, a theoretical means for improving the thermodynamic efficiency of gas turbine engines. Compared to conventional gas turbine combustors which experience a pressure loss across the combustor, RDEs offer the potential of increasing the pressure through detonation without the need for extracting additional work from the compressor. RDEs rely on a continuous detonation wave, or waves, propagating around a cylindrical annulus as it consumes a detonable fresh fuel and oxidizer mixture, as shown in Figure 1. The detonation waves travel at supersonic speeds creating a complex flow field [1]. In order to study the unsteady behavior of the detonation waves, high-speed images and temporal data from sensors such as ion probes and pressure transducers can be captured. For each sensor type, a variety of data analysis techniques have been developed and employed across the RDE community. However, as RDEs progress towards an applied technology, there is a greater need for real-time diagnostics that offer operational insights during RDE operation. High-speed imaging of RDEs typically requires extensive post-processing to provide useful information but has recently been advanced towards real-time speeds

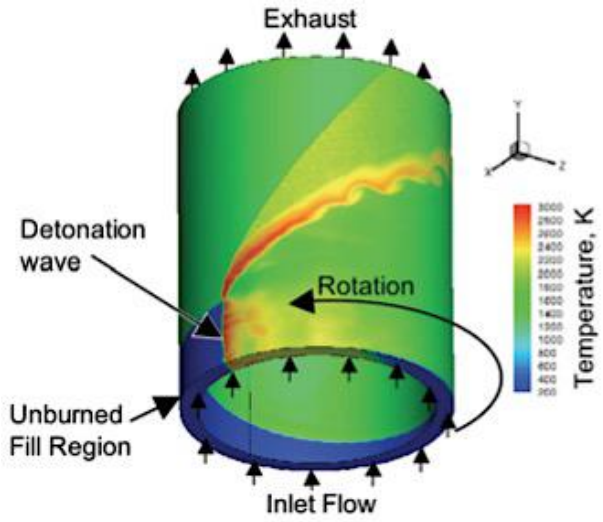

Figure 1: RDE general characteristics [1]

via Computer Vision techniques [2]. Similar to images, RDE time series data such as pressure and ion probe data offer features that suggest the active wave mode within the RDE. In many cases, those experimental data trends and features are visually intuitive to the experienced practitioner but are difficult or impossible to represent by a deterministic or analytical solution. As time series point measurements are widely common in research and across many industries, extensive work has been completed to develop more efficient means of analysis using deep learning approaches. The current study aims to build on the recommendations of that progress through the training of a series of time series classification (TSC) networks which can classify the number and direction of waves within the RDE using univariate and multivariate pressure and ion probe datasets. Each dataset will span a range of experimental conditions and time frames, but with varying dimensionality, probe selection and normalization. The unique datasets will each be used to train three networks: a residual network (ResNet), an encoder, and a fully convolutional neural network (FCN). The effects of dataset size, probe selection, data treatment, and network selection will be investigated through comparison of network performance according to classification accuracy, classification speed and viability of real-time diagnostic integration. The final selected network may then be applied to live pressure data collected via the PyDAQ package within Python, and used as a real-time diagnostic offering wave classification during experimental RDE operation.

Background

Within the RDE community, techniques analyzing optical and temporal data are utilized to classify and study the behavior of detonation waves within the RDE annulus. Both data types offer different benefits, complexities, and potential longevity throughout future RDE technology maturation. Down-axis images are commonly used to track detonation wave propagation through time by concatenating polar pixel intensities to generate *Detonation Surfaces* or *X-t* plots [3-5]. These methods offer information on the wave number, direction, and velocity. Transverse images, those captured perpendicular to the annulus center axis, have been captured via chemiluminescence to study parasitic combustion and shock structure [6,7]. In each of the mentioned studies, as well as many other experimental RDE facilities including the current study utilizing the National Energy Technology Laboratory (NETL) RDE, images are captured with high frame rates at or above 50 kfps, resulting in a wealth of images which are computationally expensive to analyze at length. For this reason, the conventional methods previously mentioned cannot be considered for real-time diagnostic purposes, which are believed to be a vital component to the continued development of RDE technology towards active control and eventual turbine integration.

In an effort to address the need for more high-speed diagnostics which can be operated in real-time, computer vision techniques, a subset of machine learning, have been applied by the current authors to down-axis RDE images for image classification and object detection in several studies. The first, which surveyed five convolutional neural network (CNN) architectures for image classification, found the number and direction of waves within an RDE annulus can be classified by a SqueezeNet architecture [8] for a single image at accuracies exceeding 98% with a classification rate exceeding 33 frames per second [9]. Extending the output capabilities of computer vision applied to down-axis RDE images, an object detection CNN architecture, You Only Look Once (YOLO) [10], was trained to detect and annotate each wave within a single image. The locations of each wave can be tracked through time to determine frame-to-frame wave velocity but at a lesser classification speed than SqueezeNet [11]. A secondary method for integrating the image classification CNN with a simplified pressure data correlation is currently being developed for real-time experimental usage with preliminary estimates wave number, direction, and speed with diagnostic feedback at 3-5 Hz.

Although the previous and ongoing machine learning approaches to RDE imaging are promising and offer significant reduction in computational time, their application beyond an experimental phase of RDE development may be limited by equipment availability and optical access. While this is not an immediate concern as experimental RDEs are expected to be studied for many years to come, it does highlight the need for a similar machine learning application to data more readily available in a turbine-integrated arrangement. It should be noted that like optical techniques, temporal data analyses have been studied at length within the RDE community. Time series data from pressure probes, ion probes, and other diagnostic have been analyzed to determine wave modes and dynamics by way of fast Fourier transform, auto-correlation, cross-correlation and other methods [3,12-16]. However, consideration of temporal data is done alongside or verified by optical techniques which offer the confidence of spatial resolution. The current study aims to fully incorporate the advantages of imaging certainty by creating a labeled dataset of input-output pairs where pressure data serves as an input and wave mode classification derived from down-axis images serve as the corresponding output. These datasets will be used to develop a collection of TSC networks.

Time series classification is a longstanding challenge in data mining which aims to probabilistically determine the correct label of univariate or multivariate time series. Univariate datasets can be generalized as a collection of vectors

containing data from a single sensor throughout time. Multivariate datasets are structured as matrices where in addition to the dimension of time, a second dimension is added for the inclusion of additional sensors. This data structure is illustrated in Figure 2. As an example, a univariate datapoint with a sample length of 200 samples would have dimensions of 1x200, while a multivariate datapoint of equal sample length that includes two sensors has dimensions of 2x200. As the number of sensors increases, so does the size of the multivariate set by stacking traces recorded simultaneously along the time axis. In the current study, as is the case in many TSC efforts, the benefit of multivariate datasets is a result of added spatial resolution as well as varying sensor type. Due to the prevalence of time series data in a wide range of fields, a vast number of methods to solve time series classification have been developed and considered. Some examples of popular and traditional solutions included nearest neighbor (NN) classifiers joined with a distance function, decision tree, support vector machines (SVM), HIVE-COTE [17], and many others [18]. With increased accuracy, however, the time complexity of each traditional method increases significantly sometimes to the point of impracticality. Therefore, Deep Learning, which has revolutionized computer vision and has shown success in natural language processing (NLP) and speech recognition, is considered as an alternative solution for TSC. In this study, deep neural networks (DNN) will be used to perform TSC on experimental RDE pressure data recorded at 250 kHz. Multiple datasets will be created to determine the advantages of univariate and multivariate time series. The DNN will work according to the DNN TSC framework shown in Figure 2. The time series, either univariate or multivariate is fed to the DNN which performs non-linear transformations according to the prescribed architecture resulting in a probability distribution over the classes present in the dataset.

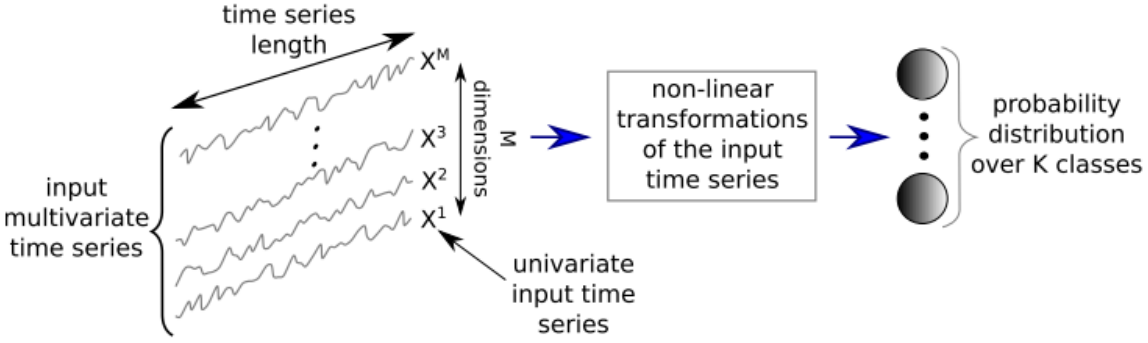

Figure 2: Generic DNN TSC framework for multivariate time series [18]

While the use of a TSC for experimental RDE data is novel, the increasing benefits of machine learning techniques have been utilized in a variety of studies across the combustion community. As a very early example, Santos-Victor et al. [19] showed that flames within a glass furnace can be classified via computer vision to determine the number of active burners as well as the reactant flow rate. Neural networks were applied in the field of gas turbines though the work of Tong et al. [20] where the effectiveness of using machine learning to predict core sizes of high efficiency turbofan engines was displayed. Grogan and Ihme [21] investigated the probability of predictive parameters for irregular combustion regimes and detonation sensitivity to heat release with machine learning. With possible application to RDEs, Barway et al. [22] presented a data-driven approach to combustion regime classification within the complex structure of detonation waves using artificial neural networks. As previously mentioned, the current authors have leveraged CNNs for RDE image classification [9], and object (wave) detection [11] as efforts contributing to the development of an RDE real-time diagnostic portfolio. Using a different data mining technique, Rezzag [23] et al. investigated instantaneous detonation wave speeds in post-processing using k-means clustering. The current work further extends the usage of CNNs within pressure gain combustion via a heavy reliance on the broader collection of previous machine learning development efforts.

Experimental Setup

Data for this study was collected from experiments conducted in the water-cooled, ducted-exhaust RDE which is fully integrated within the Low Emission Combustor Test and Research (LECTR) facility at the National Energy Technology Laboratory (NETL). A graphic of the experimental rig is shown in Figure 3, and a cross-section in Figure 4. Water-cooling of the RDE along with a portion of the exhaust permits operating the system for an indefinite period of time at fuel-lean conditions. Test duration is typically limited to 20-30 seconds in order to conserve fuel. The exhaust duct immediately following the RDE has an internal diameter of 154 mm and is water-cooled for a length of approximately 3.8 m. Here water-cooling gives way to a refractory-lined duct with an increase in diameter to 273 mm for approximately 1 m through the sampling cross. At the exit of the cross, the refractory-lined duct increases in diameter to 431 mm for approximately 1.84 m before gradually decreasing in diameter to 216 mm. The exhaust flow passes through a secondary cross, which permits fine tuning of the system backpressure (valve not shown), before encountering the primary back-pressure control valve (Valtek Mark One globe control valve), which is located approximately 7 m downstream from the RDE exit. The valve provides a means of simulating downstream loads from components such as a turbine, as well as controlling pre-combustion pressure in the RDE combustion channel independent of the RDE exit nozzle [24, 25]. Downstream of the primary control valve the flow continues through pipe of length 216 mm before passing through an exhaust muffler, irrelevant back-pressure, before leaving to the atmosphere.

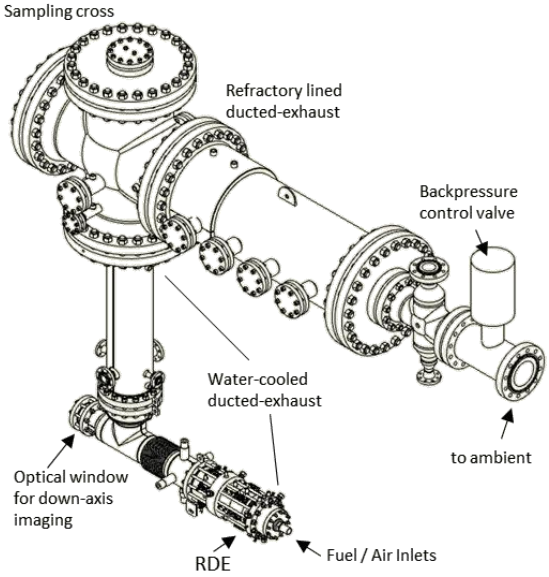

Figure 3: High-pressure, water-cooled, ducted-exhuast RDE at NETL

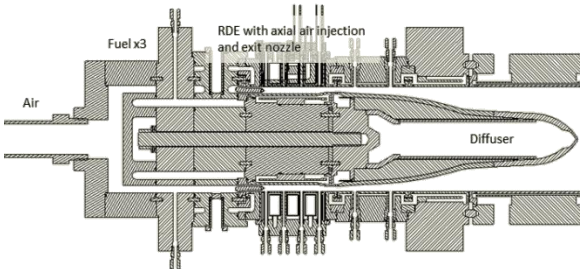

Figure 4: Profile view of water-cooled RDE showing axial air injection, sampling ports and downstream diffuser

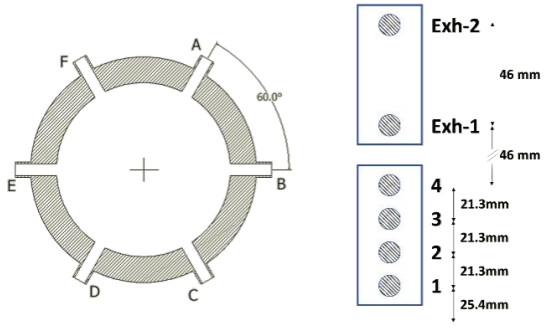

Figure 5: Nomenclature for circumferential and axial sampling locations

Combustion air is provided by an on-site compressor capable of providing a maximum flow of 1 kg/sec at a pressure of 1.4 MPa. A separate natural gas-fired air heater (1.17 MWth) can heat the air to a maximum of 600 K, although excessive heating reduces the allowable run times due to limits on vessel temperatures. The RDE is fueled by hydrogen or mixtures of natural gas and hydrogen, which are available at maximum flow rates of 55 g/s and 13 g/s, respectively. All gas flows are metered individually by Coriolis meters located approximately 3 meters upstream of the RDE inlet. Although the Coriolis meters are not capable of measuring the dynamic response of the flow at the RDE injector, they do provide an accurate (< 0.5%) measure of the flow, sampled at 5 kHz. A natural gas-air burner is located approximately 0.5 m downstream from the exit of the RDE to prevent a combustible mixture building in the exhaust duct during start-up or in the event of blow-out in the combustor. This burner also provides ignition of the RDE, as opposed to a commonly used detonation tube, as the combustion wave quickly transitions to detonation for the conditions considered in this study. Control of the facilities is provided through an Allen Bradley (AB) control system while high-speed data acquisition is performed by a National Instruments PXIe 1082 chassis with multiple analog input/output cards using a custom National Instruments LabView program. The AB records facility operating conditions at critical temperatures at a sampling rate of 1 Hz, while the NI hardware samples at rates ranging from 5kHz to 1 MHz depending upon the desired signal.

Four sample ports are located along the length of the RDE and two just downstream of the RDE exhaust at six circumferential locations as shown in Figure 5. These sample ports are used for both Infinite Tube Pressure (ITP – PCB model CA102B06) and Capillary Tube Averaged Pressure (CTAP – Omega PX309-100G5V), as well as ion probe data and band-pass OH chemiluminescence. Specific locations of parameters relevant for this study are detailed later. Down-axis images are captured at 60,000 fps by the imaging system in which a Nikkor 105 mm UV lens is used with a *Vide Scope VS4-1845HS-UV* intensifier and a Photron FASTCAM SAZ high-speed digital camera through a 3.5-inch diameter quartz viewport. Images are acquired with a resolution of 512 x 512 pixels.

The objective for this test series was to collect data at as many wave modes as permitted by the RDE. To accommodate this requirement, a range of operating conditions, detailed in Table 1, were tested across multiple RDE configurations, summarized in Table 2. The dataset includes data from both radial AFRL-style, and axial pintle/"sting" injectors, both depicted in Figure 6. Tests with the radial injector geometry included variable air injector areas as outlined in Table 2. Station designations as defined in [27] are illustrated in Figure 7 for the axial air injection RDE used in this study. The radial air injection RDE has similar station designations. These stations provide convinent reference locations for area ratio comparisons including an air injection area to combustor channel area ($A_{3.1}/A_{3.2}$) and nozzle exit area to combustor channel area ($A_8/A_{3.2}$).

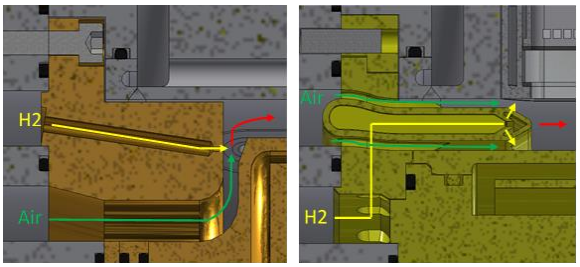

Figure 6: Radial and axial air injectors utilized in this study. Radial injector geometry was also changed as per Table 2

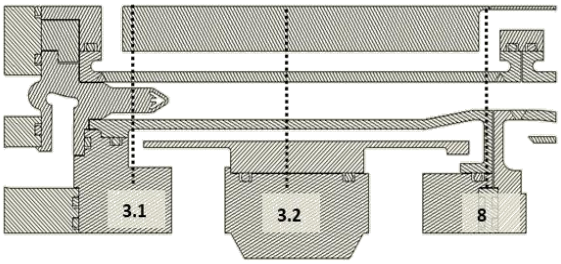

Figure 7: Water-cooled RDE with station designations at the air inlet minimum area (3.1), combustion chamber area (3.2) and nozzle throat (8) [27]

Table 1: RDE operating conditions utilized for this study

Air mass flow rate	0.52-0.7 kg/sec
Equiv. Ratio	0.5 – 0.9
Pressure (Pre-Combustion)	0 – 310 kPa
Temperature (Inlet Air)	340 – 480 K

The currently installed RDE has an outer diameter of 149-mm, a combustion channel width of 10 mm and a length of 119.5 mm. At the end of the combustor is an exit nozzle, which applies back pressure in the channel to enhance detonation. As previously noted, the RDE utilizing an axial air injector is similar to the Purdue University "Sting" injector [26]. This configuration permits axial air flow along both sides of the injector with fuel injection occurring through 120 rearward-facing angled orifices on each side of the sting injector tip, each with a diameter of 0.75 mm, providing a total fuel injection area of 106 mm^2. While not a focus of the current research study, a water-cooled diffuser is installed just downstream of the RDE exit nozzle for future study of turbine integration, and is shown in Figure 4.

Data treatment and network training are performed using NETL's cloud computing facility, WATT. WATT is a part of the NETL Center for Artificial Intelligence and Machine Learning (CAML), offering 24 40-core Intel Skylake nodes (384 GBs of RAM and four Nvidia P100 GPUs), and 40 PBs of raw storage. WATT hardware achieves 50 TFLOPs performance across all CPUs, and 323 TFLOPs performance across GPUs. The OpenStack software platform enables deep learning training and consideration of large datasets, tailored to the exploration of problems in machine learning such as the current study [28].

Table 2: Geometric variations of the RDE utilized for this study

Combustor	RDE Diameter inner/outer (mm)	Combustor Gap Size (mm)	Air Injector Area (mm2)	A3.1/A3.2	A8/A3.2
AFRL-1	134 / 149	7.5	306	0.1	1
AFRL-2	134 / 149	7.5	679	0.2	1
AFRL-3	134 / 149	7.5	1086	0.33	1
Sting Inlet	129 / 149	10	1,623	0.37	0.76

A3.0-Fuel Inlet Area, A3.1-Air Inlet Area, A3.2-Combustor Annulus Area, A8-Exit Nozzle Area

Methodology

A. *Dataset Creation and Normalization*

In order to train a TSC network, a dataset must first be established. To explore the effects of data quality, dimensionality, and length, a series of datasets are created using previously recorded experimental RDE data. Data used throughout the study, is recorded from an Ion probe and PCB, at port locations C1 and D1 respectively, according to the nomenclature described by Figure 5. Each dataset is normalized using Z-normalizing, also referred to as Z-score. Z-normalization, or standardization, centers a dataset at mean 0 with a resultant standard deviation of 1. This standardization is a common option in data treatment for deep learning, as it improves learning capabilities by presenting data features as a normal distribution. The Z-normalization, $x_{i,z}$, of data point x_i is performed using Equation 1 where μ_{global} and σ_{global} are the global mean and standard deviations of the training and validation data sets, respectively.

Example windows of Ion and PCB traces across 200 samples which are Z-normalized signal, with an overlaid example down-axis image used to classify wave mode are plotted in Figure 8.

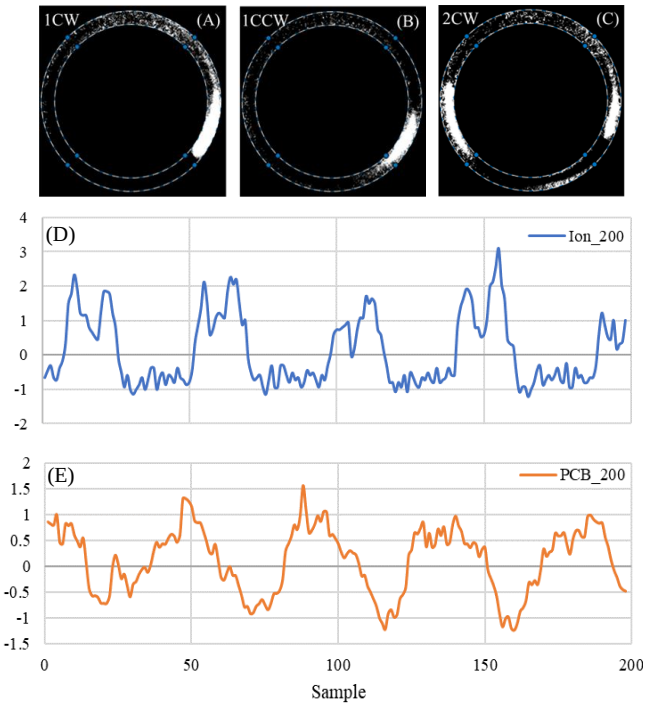

Figure 8: Example Down-axis images (A-C) and example Ion (D) and PCB (E) traces Z-normalized throughout a 200-sample window

As will be detailed in the next subsection, the DNN architectures considered include only end to end networks, therefore requiring labeled datasets. In order to create each dataset, denoted as the Dataset phase in Figure 9, windows of pressure and ion probe data are labeled according to the wave mode determined by imaging methods, either detonation surface or by image classification CNN [3,9]. Generating labels for time series data using down-axis imaging supplies modal certainty to labeling that is otherwise complicated by complex wave modes when solely considering time series data. The datasets span operating windows that include 13 wave modes, simple and complex, experienced in the water-cooled NETL RDE. Wave modes included in the datasets are: 1CW, 1CCW, 2CR, 2CW, 2CCW, 3CR, 3CW, 5CR, 6CR, 6CCW, 7CCW, 7CW, 7CR with naming convention of wave count followed by directional indicator. Directions include clockwise (CW), counterclockwise (CCW), and counter rotating (CR). In the case of CR modes, the wave number indicates the number of counter-rotating pairs. Like all classification algorithms, the DNNs will only accurately classify data according to the labels present in the dataset. Therefore, the datasets must adequately sample every expected wave mode in a variety of operating conditions. The current dataset does not wholly survey every wave mode experienced in the RDE of interest, but adequately covers complex wave behaviors and multiplicity to study the proposed application of TSC. Resulting networks will offer the ability to properly identify co- and counter-rotating wave modes, which is critical to the previous and the current work. Future work will include expanding the dataset to include additional wave mode labels.

$$x_{i,z} = \frac{x_i - \mu_{global}}{\sigma_{global}} \tag{1}$$

Univariate datasets are composed of time series having lengths of 200, 500, and 700 samples from pressure data or ion probe data. Multivariate datasets are composed of ion probe data in conjunction with pressure data with sample lengths of 200 and 500 samples. This results in 8 datasets (6 univariate, and 2 multivariate) uniquely representing a variety of detonation behaviors. To each of these datasets, three types of DNNs are applied: residual network (ResNet), encoder, and fully convolutional neural network (FCN). This parametric method will result in 24 trained networks offering insight to the benefits of various time series treatment and training aspects. Resultant recommendations can then be made regarding the future use of TSC applied to RDE data for real-time diagnostics. In order to develop a collection of networks whose performance can be compared equitably, a strict network development method is followed.

B. *Network Development*

According to the dataset composition previously outlined, 6 of the datasets will be univariate while the remaining 2 datasets will be multivariate. In both cases, the method to develop each TSC DNN is conducted according to the flowchart in Figure 9. Each DNN considered is a discriminative, end-to-end network. This simply means the networks learn from input-output pairs, and are domain agnostic, removing bias of feature engineering. Therefore, the current method is universally applied and includes four major phases: Dataset, TSC DNN Training, TSC DNN Validation, and Inference.

While the Dataset phase is only performed once for each unique dataset, the remaining three phases must be performed to produce each of the 24 trained networks. In preparation for the TSC DNN Training phase, the chosen labeled time series dataset, whose generation was outlined in the previous subsection, is split into training and validation datasets with proportions of 70% and 30% respectively. Once split into respective datasets, the TSC DNN Training phase is initiated. Training data and labels from the given univariate or multivariate dataset are fed to an untrained DNN whose architecture must be determined and created beforehand with randomly initialized weights. As the network is presented with the dataset, parameterized weights are internally updated using a backward pass to propagate the error of model prediction through gradient descent. Simultaneously, the TSC DNN Validation phase is being performed to evaluate validation loss. In this process, the validation dataset is fed to the incrementally updated TSC DNN without labels. Each time the network is exposed to all data, an *epoch* is completed. For the current study, all network iterations are trained for 250 epochs. Once the network's training loss is minimized alongside the validation loss, the DNN is considered a trained and validated network. This training and validation process must be performed for each desired network-dataset combination.

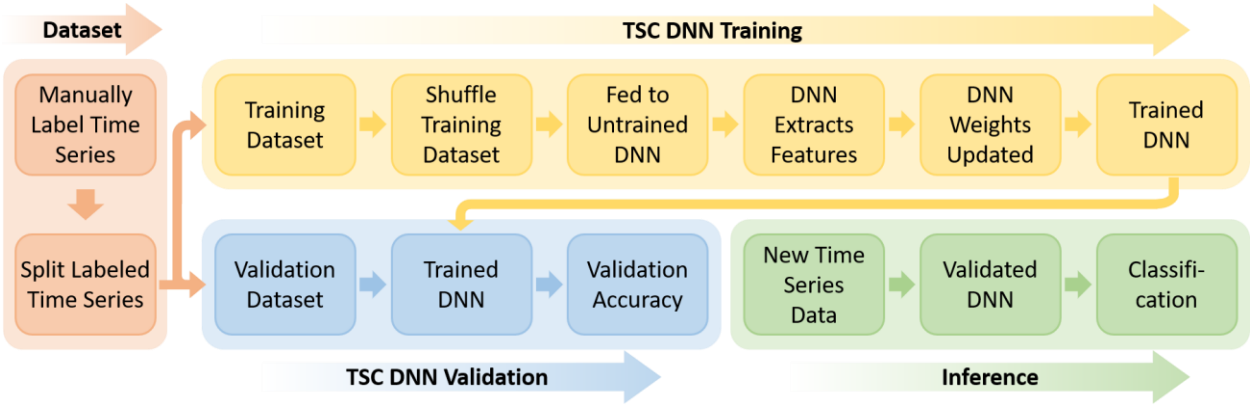

Figure 9: TSC DNN Development Method Flowchart

C. *Network Selection and Usage*

In an effort to obtain the most high-performing model, the training process is reinitialized and completed five times for each network, each time with newly randomized initial weights. Across the five iterations, a "best model" is retrieved and saved for end usage. The best model is not often at the final epoch, but instead a previous epoch at which the parameterized weights are found to minimize loss. In each case, a categorical cross-entropy loss function, also called SoftMax loss, is used to determine the best model among the five iterations. Categorical cross-entropy is a measure of similarity between two probability distributions. For classification problems, these are the incremental network's output of a probability distribution for each label and the labeled data. In other words, for each classification attempt, the network outputs a probability distribution vector of length equal to the number of possible classifications. The maximum probability within the distribution determines the output label, which is compared to the label provided by the dataset generation process. The loss function can be optimized by stochastic gradient descent (SGD) and is a low cost and effective choice for classification networks [29].

A broad range of DNNs and an even larger selection of more traditional classifiers in categories such as NN or SVMs are available to train for the proposed study. The selection of deep learning architectures, based on their advantageous simplicity and previous successes in efforts similar to TSC, somewhat narrows the selection of potential architectures. To address a similar issue, Fawaz et al. [18] surveyed eight popular and proven methods in their ability to classify univariate and multivariate publicly available timeseries repositories [30, 31]. Fawaz ranked architecture performance with respect to themes, dataset length, and training size. In each category corresponding to the current study (Theme: Sensor, Length: 251-700, Train size: >799), the top three performing networks were the same. Those networks, Encoder, FCN, and ResNet, are therefore chosen for the current study and will be briefly summarized.

The Encoder architecture is a computationally lightweight hybrid structure, whose output is summarized by a convolutional attention layer. The architecture begins with three convolutional blocks with max-pooling layers between each. Within each convolutional block is an instance normalization fed to a parametric rectified linear unit (PReLU) activation function, thought to be a possible improvement on the widely used rectified linear unit (ReLU) activation [32]. This varies from the somewhat similar FCN architecture, which relies on a global average pooling (GAP) layer instead of the encoder's attention layer. Both have three convolutional layers, but within the FCN convolutional block is a batch normalization fed to a ReLU activation function [33]. The ReLU activation function has brought much success to deep learning by overcoming the vanishing gradient issue associated with sigmoid and hyperbolic tangent activations. The final architecture, ResNet, is specifically designed to address the degradation problem where deeper networks experience saturated accuracies and become less effective than more shallow networks. This is accomplished by the residual block, depicted in Figure 10, which relies on a skip connection supplying information from earlier layers that would otherwise become too abstract [35]. The ResNet used in this study contains nine convolutional layers followed by a GAP layer [33]. Although the complexities and purposes of each network may seem dissimilar, they are all trained according to the method depicted in Figure 9.

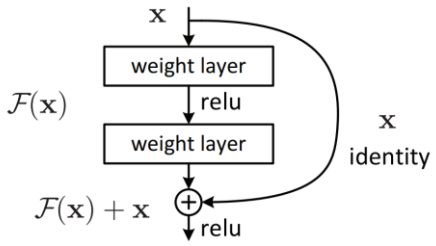

Figure 10: Generic ResNet residual block [34]

The resulting best network(s) can then be used indefinitely within the Inference phase to classify the wave mode from new experimental timeseries data. Each trained network is only applicable to data arrangements identical to that of the initial training data, and viable for wave modes included in the training labels. To adapt the network to a new data arrangement or additional wave modes, the network development methodology can be applied from scratch, or transfer learning may be applied in some instances. Otherwise, the phase of Inference can be utilized as a TSC tool indefinitely.

For application as a real-time diagnostic technique, the networks may be used to classify "live" experimental data within the RDE lab environment. Using the PyDAQ package within Python, data windows can be collected from the appropriate sensors, and passed through the chosen TSC DNN. Similar to the technique proposed as an extension to the previous image classification study [9] whose findings will be published in a future work, the DNN output of wave number and direction can drastically simplify calculation of other wave metrics. To generate diagnostic information, the same short window of sensor data fed to the DNN can be analyzed through a simple correlation method to determine wave speeds and frequencies. Informed of the wave mode via DNN output, the correlation, which is computationally cheap, can determine individual wave frequencies and velocities. This diagnostic output data, provided by the TSC and subsequent correlation method, is similar to that of an FFT but requires much less data while offering modal certainty that is otherwise elusive in time series dataset absent of optical verification. A second option, which may be considered in future work, combines the output of the current DNN with parameters derived through feature engineering of the time series signal. Each parameter, being fed to a regression network, could be used to estimate wave speed and frequency.

Results

Three DNN architectures were trained on 8 unique datasets (6 univariate and 2 multivariate). Univariate datasets include data from either an ion probe or pressure reading at sample lengths 200, 500, and 700 samples. Multivariate datasets are made up of simultaneous ion and pressure data at sample lengths of 200 and 500 samples. Each dataset is labeled with wave modes extracted from down-axis high speed images. This combination results in 24 unique finalized networks. Finalized networks represent the model that best minimized categorical cross-entropy loss throughout five random initializations, with training durations of 250 epochs each. Results for the 24 models, including training accuracy, validation accuracy and classification time, are summarized in Table 3 below. Training and validation accuracies measure the model's ability to classify data windows from the training and validation datasets, respectively. Classification time, reported in milliseconds, is the time it takes the model to analyze and predict a label for a single data window. Classification times reported in Table 3 are an average of 10 consecutive classifications. Intuitively, lesser classification times are preferred for downstream usage within a real-time diagnostic.

Table 3: Results for tested CNN architectures

Architecture	Dimen-sionality	Data Length	Data Type	Training Accuracy	Validation Accuracy	Classification Times [msec]
Encoder	Univariate	200	Ion Probe	99.52%	77.56%	32.09
	Univariate	200	PCB Data	99.25%	71.44%	32.13
	Univariate	500	Ion Probe	99.94%	74.21%	33.78
	Univariate	500	PCB Data	99.92%	67.86%	33.64
	Univariate	700	Ion Probe	99.94%	71.88%	38.90
	Univariate	700	PCB Data	100.00%	66.12%	39.06
	Multivariate	200	Ion and PCB Data	100.00%	94.51%	35.77
	Multivariate	500	Ion and PCB Data	100.00%	88.13%	44.33
FCN	Univariate	200	Ion Probe	98.54%	82.62%	28.29
	Univariate	200	PCB Data	98.45%	73.26%	28.21
	Univariate	500	Ion Probe	97.57%	84.12%	29.07
	Univariate	500	PCB Data	96.02%	76.83%	29.11
	Univariate	700	Ion Probe	97.17%	87.23%	30.02
	Univariate	700	PCB Data	94.12%	82.58%	31.18
	Multivariate	200	Ion and PCB Data	100.00%	91.36%	28.76
	Multivariate	500	Ion and PCB Data	100.00%	89.89%	29.71
ResNet	Univariate	200	Ion Probe	99.95%	87.63%	36.25
	Univariate	200	PCB Data	99.98%	83.08%	39.10
	Univariate	500	Ion Probe	99.95%	87.63%	31.74
	Univariate	500	PCB Data	99.97%	86.63%	31.83
	Univariate	700	Ion Probe	99.91%	89.85%	32.65
	Univariate	700	PCB Data	100.00%	87.40%	33.21
	Multivariate	200	Ion and PCB Data	100.00%	94.24%	32.50
	Multivariate	500	Ion and PCB Data	100.00%	88.35%	31.66

Generally speaking, a majority of the models achieve accuracies that may be suitable for end usage absent of competition. Additionally, the three architectures appear to each be competitive in various aspects. On average, ResNet achieves higher validation accuracies while the encoder achieves the highest accuracies by a single network. The FCN network demonstrates overall higher accuracies than the encoder with better classification times. One consistent trend across each architecture is a higher performance on multivariate datasets, which will be further explained later in this section. Competing metrics between the three architectures highlight the absence of a clear optimal model choice or preexisting "formula" for model design for a given dataset. Effects of network depth and other design choices may suggest performance abilities to an experienced user. However, it is never fully known how one network may outperform another for any new dataset, and therefore a parametric comparison of various networks is necessary. Although the final results of the differing architectures seem incredibly similar, the progression of their learning process demonstrates the existence of their internal differences, which were detailed in the previous section. Training accuracies are plotted against epochs for encoder, FCN and ResNet networks trained on univariate datasets in Figures 11, 12, and 13. Training accuracies for all multivariate networks are plotted in Figure 14 below.

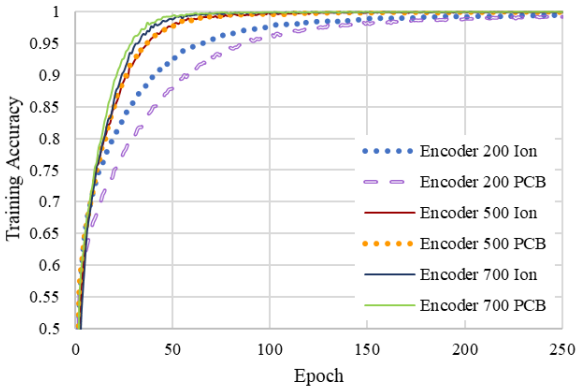

Figure 11: Training Accuracy for Univariate Encoder Networks versus Epochs

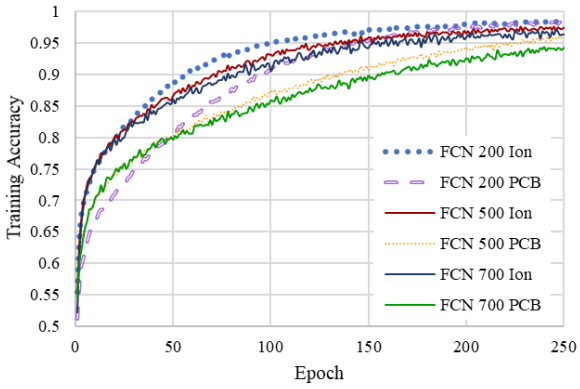

Figure 12: Training Accuracy for Univariate FCN Networks versus Epochs

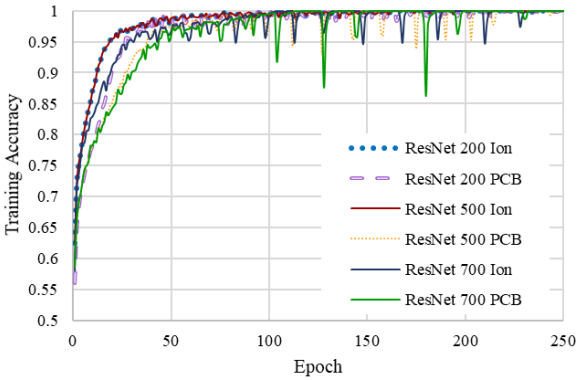

Figure 13: Training Accuracy for Univariate ResNet Networks versus Epochs

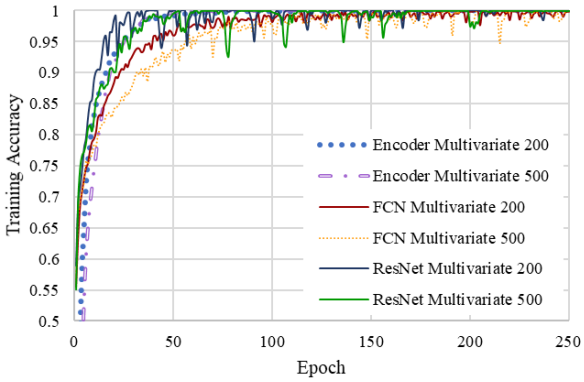

Figure 14: Training Accuracy for Multivariate Networks versus Epochs

A multitude of behaviors can be observed in the above trends but will be discussed briefly as this is intended to be a demonstration of development of DNNs as tools for end-usage in a lab environment. In Figure 11, it is shown that the encoder responds more quickly to longer data windows. For a given data length, the encoder does not consistently favor ion or pressure data. This is not true for the other univariate networks which all favor ion probe data. Higher accuracies associated with ion probe datasets are expected as a result of the more prominent trends in ion traces compared to the lesser quality of the pressure data, illustrated in Figure 8. Figure 12 highlights FCN networks' more gradual learning with the most prominent performance gap between ion and pressure data regardless of data length. Univariate ResNet achieves accuracies exceeding 95% in the fewest epochs, shown in Figure 13, but begins to overcorrect weights once the training accuracy is saturated. Each of these trends are echoed by the multivariate networks, shown in Figure 14.

Excluding the univariate encoder, all networks tend to perform better on shorter data lengths in early epochs. Without clarification, this may be incredibly counterintuitive as "less data" should contain less characteristic information. Therefore, it is pertinent to acknowledge that each dataset was created from the same pool of data, creating an exchange between data length and total datapoints. In other words, while data lengths of 500 may offer more informative features than data lengths of 200 within a single window, the latter dataset contains more than twice as many data windows with associated labels. It is likely that given an equal number of datapoints, larger data lengths would outperform their shorter counterparts with a negative impact of larger classification and data acquisition times. To study this relationship, a significant portion of labeled data would not be utilized in the shorter data length sets. This activity, wasting labeled experimental data, does not align with the current scope of work which aims to create the high-performing DNNs with the available data. To further consider impacts of sample lengths, Figure 15 shows training and validation accuracies of best models versus sample length.

While Figures 11-14 showed incremental training accuracies, Figure 15 summarizes the accuracies associated with the model that best minimizes loss, coinciding with the data reported in Table 3. In this format, the exchange between data length and datapoint volume can be further quantified for the three sample lengths 200, 500, and 700 samples. For both training accuracies, univariate and multivariate, values are so high that little to no influence is attributed to sample length. Univariate validation accuracies are very scattered, but trend somewhat upward with larger sample lengths. Simultaneously, the lowest univariate validation accuracies worsen with larger sample lengths, likely a result of lesser validation datapoint volume. The most prominent trend is associated with multivariate validation accuracy, which is negatively impacted by increasing sample size. This exchange of data length and data volume is exacerbated in the multivariate cases as a result of an overall lower data volume available where ion and pressure data were both recorded at the port locations, C1 and D1, chosen for this study. For this reason of sparsity, a multivariate dataset with sample length of 700 was not created.

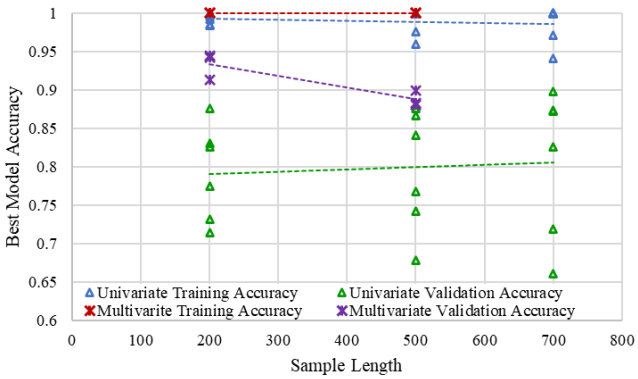

Figure 15: Training and Validation Accuracy for Univariate and Multivariate Networks versus Sample Length

Figure 15 also emphasizes the superior performance of multivariate networks over univariate at every sample length. Multivariate lengths of 200, having dimension of 2x200 equivalent to a reshaped 400 data length, outperform univariate lengths of 500 from a lager data pool. Again, this may seem illogical, but can be accounted for in the physical understanding of the sensor locations. Both sensors are located at axial locations closest to the detonation plane, or the base of the RDE. They are circumferentially separated by 60°, offering some degree of spatial variation in the data fed to the DNNs. Like any correlation method, information representing detonation behavior at various locations within the annulus greatly clarifies the wave mode. It is expected that a multivariate set where two sensors are circumferentially aligned and axially spaced would experience a lesser benefit as the additional spatial information would only respond to more vague behaviors such as wave height or combustion strength.

Beginning a process of selecting a preferred network or architecture to utilize as a real-time diagnostic component, Table 4 lists validation accuracy of each architecture and its respective rank amongst competitors for a given dataset. Validation accuracy, a measure of the network to classify unlabeled data, is the better accuracy indicator of a network's performance on new data. With data rearranged to the format below, it is abundantly clear that ResNet is the top performer for all univariate datasets. Likewise, FCN outranks the encoder in every univariate instance. For multivariate datasets, the three networks tie with an average rank of 2. Interestingly, the dataset for which the encoder achieves the top rank is the only instance of not exhibiting the lowest performance. Across all datasets, ResNet has the highest average rank of 1.25. Therefore, if TSC is to be performed on RDE sensor data with no access to supercomputing resources that allow a survey similar to that presented in the current study, ResNet is recommended to most likely achieve highest accuracies. However, a survey of architectures should be performed whenever possible.

Table 4: Performance comparison of each network for given datasets with rank

Dataset Type	**Data Source**	**Samp. Length**	**Encoder** [Val. Acc. (Rank)]	**FCN** [Val. Acc. (Rank)]	**ResNet** [Val. Acc. (Rank)]
Univariate	Ion	200	77.56% (3)	82.62% (2)	87.63% (1)
Univariate	PCB	200	71.44% (3)	73.26% (2)	83.08% (1)
Univariate	Ion	500	74.21% (3)	84.12% (2)	87.63% (1)
Univariate	PCB	500	67.86% (3)	76.83% (2)	86.63% (1)
Univariate	Ion	700	71.88% (3)	87.23% (2)	89.85% (1)
Univariate	PCB	700	66.12% (3)	82.58% (2)	87.40% (1)
Multivariate	Ion+PCB	200	94.51% (1)	91.36% (3)	94.24% (2)
Multivariate	Ion+PBC	500	88.13% (3)	89.89% (1)	88.35% (2)
Overall Univariate Rank (Avg.)			**(3)**	**(2)**	**(1)**
Overall Multivariate Rank (Avg.)			**(2)**	**(2)**	**(2)**
Overall Rank (Avg.)			**(2.75)**	**(2)**	**(1.25)**

Because the current study aims to develop a component of a real-time RDE diagnostic, classification time must be optimized alongside validation accuracy. Figure 16 is used to visualize those parameters for each architecture. It can be seen that FCN boasts the shortest classification times with an overall minimum of 28.21 milliseconds (msec). ResNet, being the deepest network, experiences larger classification times in exchange for higher accuracies. In this format of consideration, the Encoder becomes a lessor competitor with lower accuracy and higher classification times.

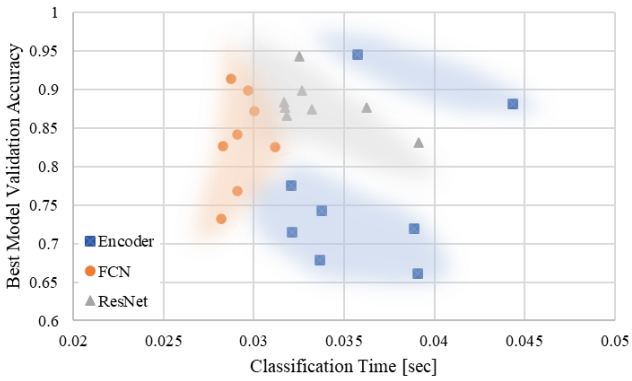

Figure 16: Validation Accuracy of three Architectures versus Classification Time

Analyzing Figure 16, two networks appear to be viable choices. The first being the highest-accuracy FCN which achieves 91.36% validation accuracy and 28.76 msec classification time. The second choice is the highest-accuracy ResNet demonstrating 94.24% validation accuracy and a classification time of 32.50 msec. Consistent with the trends previously discussed, both contending networks are multivariate with data lengths of 200. Therefore, data acquisition setup and time are not deciding factors. Because validation accuracies of both options are very similar, the multivariate 200 sample length FCN network, also highlighted in Table 3, is chosen over the ResNet for the improved classification time. While less than 3% difference in accuracy is not expected to create drastic effects, a 13% slower ResNet may hinder real-time capabilities. At the chosen network's classification speed, new classifications can be generated at just under 35 Hz, which exceeds current capabilities.

As a preliminary exercise of real-time diagnostic calculations, previously recorded Ion probe and PCB data were fed to the finalized network. The TSC classification output, which includes wave number, was utilized by a simplistic correlation method. Across 100 windows, each spanning 200 samples like the example traces in Figure 8, an average frequency and individual wave speed of 5556.6 Hz and 1298.8 m/sec were calculated, respectively. This frequency compares well to a frequency of 5617.3 Hz found using an FFT across 20,000 samples with a resolution of 61 Hz. In addition to calculations requiring much fewer samples, the TSC output provides wave number and directionality, which is typically estimated using a comparison of wave frequency proportional to the theoretical Chapman-Jouguet (CJ) velocity. Those estimations are further complicated by complex wave behaviors such as counter-rotating waves. The output of the TSCs developed in this study circumnavigate the CJ comparison in its entirety, resulting in an individual wave speed calculation at each iteration. Calculations of frequency and wave speed consume an average of 0.041 msec per iteration, barely impacting the diagnostic feedback rate. This exercise largely resembles diagnostic implementation in the lab environment, lacking only the addition of live data acquisition. Due to time constraints, full integration of the diagnostic with live experimental data acquisition will be performed as future work. However, the validity of TSC-output-informed correlation has been demonstrated by this preliminary exercise. Only the final diagnostic feedback rate will be affected due to the additional, but presumably small, data acquisition time per iteration. In the unexpected case of large data acquisition times, a univariate TSC may be preferred.

Fortunately, finalized network files and inference execution are formatted to be easily interchangeable if lab integration shifts preferences of accuracy and classification time. Additional future work will include consideration of non-DNN machine learning algorithms identified as potential means to further reduce classification time, and therefore increase diagnostic feedback. It is worth noting that almost all FCN networks, including the preferred network, outperform the reported classification time of SqueezeNet, 29.9 msec, when applied to RDE images for image classification in a previous work. Although SqueezeNet is optimized for time, the total data within a single image is drastically larger than the sensor data used for the current TSC method. That larger data volume, however, offers more spatial resolution, resulting in a higher validation accuracy of 98.5% [9]. Paired with reduced acquisition time compared to imaging, during live RDE monitoring, the developed TSC method should prove a useful diagnostic tool and give further insight into the benefits of machine learning within the PGC community.

Conclusion

In an effort to develop a functional component of a real-time RDE diagnostic, a multitude of deep neural networks (DNNs) were trained for time series classification using pressure and ion probe time series data collected from the NETL water-cooled RDE. Data labels were generated using down-axis high-speed imaging methods. Labels indicate the number and direction of detonation waves within the RDE annulus, or the wave mode, and include 13 unique wave modes in total. Labeled time series data was then used to generate 8 datasets, of which 6 were univariate with lengths of 200, 500, and 700 samples, consisting of either ion or pressure data. The 2 remaining datasets were multivariate with lengths of 200 and 500 samples, containing simultaneous ion and pressure data. Each dataset was used to train three time series classification (TSC) DNN architectures, being an encoder, an FCN, and a 10-layer ResNet. This combination resulted in 24 final networks, each of which were optimized by a categorical cross-entropy loss function.

Training accuracy, validation accuracy, and classification time were reported and compared against epochs, data lengths, and one another for each finalized network. Various trends within the network performance analysis as well as recommendations for network selection and future implementation were presented. Excluding the univariate encoder, all networks more quickly responded to shorted data lengths, due to the increase in total data points and labels. Finalized training accuracies of multivariate networks responded most negatively to an increase in data length. In every case, multivariate networks outperformed univariate networks due to the added benefit of spatial resolution. When comparing the ranks of the three architectures, ResNet achieved the highest overall average rank of 1.25. For this reason, any new studies which must be performed in the absence of a DNN survey due to a lack of computational resources are recommended to start with a ResNet architecture. Otherwise, a survey of DNNs should be conducted for any new dataset to determine the network best suited for the parameters of highest interest.

Within the current study, which aims to develop a TSC network as a component of an RDE real-time diagnostic, classification time was of highest importance when comparing networks. According to these priorities, a network with a slightly lesser accuracy than the highest-accuracy network was chosen for its 13% faster classification speed. An FCN trained on the 200 data length, multivariate ion and pressure dataset was chosen with final training accuracy, validation accuracy, and classification time of 100%, 91.36%, and 28.76 msec, respectively. A classification time of 28.76 msec, which corresponds to the time needed to predict a label for a new data window, results in a classification frequency of nearly 35 Hz, outperforming the image classification network developed in a previous study. As RDE technology progresses, and active control is developed, the required diagnostic feedback rate will become more well defined. While the presented TSC method should be further improved through future work, this new capability exceeds existing feedback rates. In combination with a smaller data acquisition time compared to that of imaging, this TSC method is expected to provide an improved means of real-time or near-real-time diagnostics within the experimental RDE environment. To perform this diagnostic, short windows of ion and/or pressure data will be collected using the PyDAQ package within Python. Live data will then be fed to a network developed by this study, which will predict a wave mode classification. That data, including the wave number and direction, are then fed to a lean correlation method that calculates wave velocity and frequency. This output information is widely available and commonly used in post-processing due to the larger data windows required by techniques like FFT. An ability to generate this information and other RDE performance metrics in real-time will be vital to the development of active control and gas turbine integration. It is believed that these goals can be met by a portfolio of artificial intelligence techniques, and that the results of the presented TSC method serve as another progressing step in the implementation of machine learning within pressure gain combustion technologies.

Acknowledgments

This work was completed within the DOE / NETL Advanced Turbines Program with Rich Dennis as the Technology Manager. Research was supported by an appointment to the National Energy Technology Laboratory Professional Internship Program, sponsored by the U.S. Department of Energy and administered by the Oak Ridge Institute for Science and Education (ORISE).

References

[1] Nordeen, C., Schwer, D., Schauer, F., Hoke, J., Cetegen, B., and Barber, T., "Thermodynamic Modeling of a Rotating Detonation Engine," *49th AIAA Aerospace Sciences Meeting Including the New Horizons Forum and Aerospace Exposition*, 2011.
doi: 10.2514/6.2011-803

[2] Johnson, K. B., Ferguson, D. H., Tempke, R. S., and Nix, A. C., "Application of a Convolutional Neural Network for Wave Mode Identification in a Rotating Detonation Combustor Using High-Speed Imaging," *ASME 2020 Turbomachinery Technical Conference and Exposition*, 2020. Need to cite our journal paper, not conference paper
doi: 10.1115/GT2020-15676

[3] Johnson, K., Ferguson, D. H., and Nix, A., "Validation of Cross-Correlation Detonation Wave Mode Identification Through High-Speed Image Analysis," *AIAA Scitech 2020 Forum*, 2020.
doi: 10.2514/6.2020-1179

[4] Bennewitz, J. W., Bigler, B. R., Hargus, W. A., Danczyk, S. A., and Smith, R. D., "Characterization of detonation wave propagation in a rotating detonation rocket engine using direct high-speed imaging," *2018 Joint Propulsion Conference*, 2018.
doi: 10.2514/6.2018-4688

[5] Bohon, M. D., Bluemner, R., Paschereit, C. O., and Gutmark, E. J., "High-speed imaging of wave modes in an RDC," *Experimental Thermal and Fluid Science*, 2019, 28–37.
doi: 10.1016/j.expthermflusci.2018.10.031

[6] Chacon, F., and Gamba, M., "Study of Parasitic Combustion in an Optically Accessible Continuous Wave Rotating Detonation Engine," *AIAA Scitech 2019 Forum*, 2019.
doi: 10.2514/6.2019-0473

[7] Athmanathan, V., Fisher, J. M., Ayers, Z., Cuadrado, D. G., Andreoli, V., Braun, J., … Roy, S., "Turbine-integrated High-pressure Optical RDE (THOR) for injection and detonation dynamics assessment," *AIAA Propulsion and Energy 2019 Forum*, 2019.
doi: 10.2514/6.2019-4041

[8] Iandola, F.N., Han, S., Moskewicz, M.W., Ashraf, K., Dally, W.J. and Keutzer, K., 2017, "SqueezeNet: AlexNet-level Accuracy with 50x Fewer Parameters and <0.5MB Model Size," *International Conference on Learning Representations 2017*, Toulon, FR, April 24-26, 2017, arXiv Paper No. 1602.07360v4.

[9] Johnson, K. B., Ferguson, D. H., Tempke, R. S., and Nix, A. C. "Application of a Convolutional Neural Network for Wave Mode Identification in a Rotating Detonation Combustor Using High-Speed Imaging." *ASME. J. Thermal Sci. Eng. Appl.* December 2021; 13(6): 061021.
doi: 10.1115/1.4049868

[10] Redmon, J., Divvala, S., Farhadi, A., and Girshick, R., "You only look once: unified, real-time object detection," *Proceedings of the Ieee Computer Society Conference on Computer Vision and Pattern Recognition*, 2016, pp. 779–788.
doi: 10.1109/CVPR.2016.91

[11] Johnson, K., Ferguson, D. H., and Nix, A. C. "Individual Wave Detection and Tracking within a Rotating Detonation Engine through Computer Vision Object Detection applied to High-Speed Images," *AIAA SciTech 2020 Forum*, 2020.
doi: 10.2514/6.2021-1382

[12] Bluemner, R., Bohon, M. D., Paschereit, C. O., and Gutmark, E. J. "Dynamics of counter-rotating wave modes in an RDC," *2018 Joint Propulsion Conference*, 2018.
doi: 10.2514/6.2018-4572

[13] Bluemner, R., Bohon, M. D., Paschereit, C. O., and Gutmark, E. J. "Single and Counter-Rotating Wave Modes in an RDC," *2018 AIAA Aerospace Sciences Meeting*, 2018.
doi: 10.2514/6.2018-1608

[14] Bohon, M. D., Bluemner, R., Paschereit, C. O., and Gutmark, E. J. "Cross-correlation as a tool for measuring RDC wave speed, direction, and complexity," *2018 Joint Propulsion Conference*, 2018.
doi: 10.2514/6.2018-4569

[15] Zahn, A., Knight, E., Anand, V., Jodele, J., and Gutmark, E. J. "Examination of Counter-Rotating Detonation Waves Using Cross-Correlation," *2018 Joint Propulsion Conference*, 2018.
doi: 10.2514/6.2018-4568

[16] St. George, A. C., Ganesh Kumar, V. A., Driscoll, R. B., and Gutmark, E. J. "A Correlation-Based Method to Quantify the Operating State in a Rotating Detonation Combustor," *54th AIAA Aerospace Sciences Meeting*, January, 2016, pp.1–15.
doi: 10.2514/6.2016-1402

[17] Lines J, Taylor S, and Bagnall A. "HIVE-COTE: The hierarchical vote collective of transformation- based ensembles for time series classification," *IEEE International Conference on Data Mining*, 2016, pp 1041–1046.
doi: 10.1109/ICDM.2016.0133

[18] Ismail Fawaz, H., Forestier, G., Weber, J., Idoumghar, L., and Muller, P. A. "Deep learning for time series classification: a review," *Data Mining and Knowledge Discovery*, 33(4), 2019, pp. 917–963.
doi: 10.1007/s10618-019-00619-1

[19] J. A. Santos-Victor, J. P. Costeira, J. A. B. Tomé, and J. J. S. Sentieiro, "A computer vision system for the characterization and classification of flames in glass furnaces," *IEEE Trans. Ind. Appl*., vol. 29, no. 3, pp. 470–478, 1993.
doi: 10.1109/28.222414.

[20] M. T. Tong, "Using machine learning to predict core sizes of high-efficiency turbofan engines," *Proc. ASME Turbo Expo*, vol. 1, no. November, pp. 1–7, 2019.
doi: 10.1115/1.4044770.

[21] Grogan, K. P., and M. Ihme. "Identification of Governing Physical Processes of Irregular Combustion through Machine Learning." *Shock Waves*, vol. 28, no. 5, Springer Berlin Heidelberg, 2018, pp. 941–54.
doi:10.1007/s00193-018-0852-y..

[22] Barwey, Shivam and Prakash, Supraj and Hassanaly, Malik and Raman, Venkat. "Data-driven Classification and Modeling of Combustion Regimes in Detonation Waves," *Flow, Turbulence and Combustion*. 106, 2021.
doi: 10.1007/s10494-020-00176-4.

[23] Rezzag, T, Burke, R, and Ahmed, K. "A Kinematic Study of Individual Rotating Detonation Engine Waves Using K-means Algorithm," *Proceedings of the ASME Turbo Expo 2021*: *Turbomachinery Technical Conference and Exposition*. Volume 3A: Combustion, Fuels, and Emissions. Virtual, Online. June 7–11, 2021. V03AT04A019. ASME.
doi: 10.1115/GT2021-58814

[24] Roy, A., Ferguson, D. H., Sidwell, T., O'Meara, B., Strakey, P., Bedick, C. and Sisler, A., "Experimental Study of Rotating Detonation Combustor Performance under Preheat and Back Pressure Operation*," 55th AIAA Aerosp. Sci. Meet*.(January), pp. 1–16, 2017.
doi: 10.2514/6.2017-1065

[25] Ferguson, D. H., O'Meara, B., Roy, A. and Johnson, K., "Experimental measurements of NOx emissions in a Rotating Detonation Engine," *AIAA Scitech 2020 Forum, American Institute of Aeronautics and Astronautics*, ORlando, FL, 2020.
doi: 10.2514/6.2020-0204

[26] Walters, I. V., Journell, C. L., Lemcherfi, A., Gejji, R., Heister, S. D. and Slabaugh, C. D., "Experimental Investigation of a Piloted, Natural Gas-Air Rotating Detonation Wave Combustor," *2018 Jt. Propuls. Conf., American Institute of Aeronautics and Astronautics Inc*, AIAA, 2018.
doi: 10.2514/6.2018-4782

[27] Brophy, C. M. and Codoni, J., "Experimental Performance Characterization of an RDE Using Equivalent Available Pressure," *AIAA Propuls. Energy 2019 Forum, American Institute of Aeronautics and Astronautics*, Indianapolis, IN, 2019.
doi: 10.2514/6.2019-4212

[28] "NETL's Private Infrastructure as a Service (Iaas) Cloud Computing Environment." Center for Artificial Intelligence and Machine Learning, https://ml.netl.doe.gov/index.html.

[29] Bonaccorso c/o Quandoo G. "Mastering Machine Learning Algorithms: Expert Techniques to Implement Popular Machine Learning Algorithms and Fine-Tune Your Models," *Birmingham: Packt Publishing*; 2018. Accessed November 30, 2021.

[30] Yanping Chen, Eamonn Keogh, Bing Hu, Nurjahan Begum, Anthony Bagnall, Abdullah Mueen and Gustavo Batista " The UCR Time Series Classification Archive," 2015, URL:www.cs.ucr.edu/~eamonn/time_series_data/

[31] Baydogan M.G., "Multivariate time series classification datasets,", 2015, URL: http://www. mustafabaydogan.com, Accessed 30 Jun 2021

[32] Serrà, Joan and Pascual, Santiago and Karatzoglou, Alexandros. "Towards a universal neural network encoder for time series," 2018, arXiv Paper No. 1805.03908v1
doi: 10.3233/978-1-61499-918-8-120

[33] Wang, Zhiguang, Weizhong Yan and Tim Oates. "Time series classification from scratch with deep neural networks: A strong baseline." *2017 International Joint Conference on Neural Networks* (IJCNN), 2017, pp. 1578-1585.
doi: 10.1109/IJCNN.2017.7966039

[34] He, K., Zhang, X., Ren, S. and Sun, J., "Deep Residual Learning for Image Recognition," *Proceedings of the 2016 IEEE Conference on Computer Vision and Pattern Recognition* (CVPR), Las Vegas, NV, June 27-30, 2016, pp. 770-778.
doi: 10.1109/CVPR.2016.90